doi:10.1038/nature09624

Glioblastoma stem-like cells give rise to tumour endothelium

Rong Wang[1,2,3], Kalyani Chadalavada[4], Jennifer Wilshire[5], Urszula Kowalik[1], Koos E. Hovinga[1,6], Adam Geber[1], Boris Fligelman[1], Margaret Leversha[4], Cameron Brennan[1,3,7] & Viviane Tabar[1,2,3]

Glioblastoma (GBM) is among the most aggressive of human cancers[1]. A key feature of GBMs is the extensive network of abnormal vasculature characterized by glomeruloid structures and endothelial hyperplasia[2]. Yet the mechanisms of angiogenesis and the origin of tumour endothelial cells remain poorly defined[3–5]. Here we demonstrate that a subpopulation of endothelial cells within glioblastomas harbour the same somatic mutations identified within tumour cells, such as amplification of *EGFR* and chromosome 7. We additionally demonstrate that the stem-cell-like CD133$^+$ fraction includes a subset of vascular endothelial-cadherin (CD144)-expressing cells that show characteristics of endothelial progenitors capable of maturation into endothelial cells. Extensive *in vitro* and *in vivo* lineage analyses, including single cell clonal studies, further show that a subpopulation of the CD133$^+$ stem-like cell fraction is multipotent and capable of differentiation along tumour and endothelial lineages, possibly via an intermediate CD133$^+$/CD144$^+$ progenitor cell. The findings are supported by genetic studies of specific exons selected from The Cancer Genome Atlas[6], quantitative FISH and comparative genomic hybridization data that demonstrate identical genomic profiles in the CD133$^+$ tumour cells, their endothelial progenitor derivatives and mature endothelium. Exposure to the clinical anti-angiogenesis agent bevacizumab[7] or to a γ-secretase inhibitor[8] as well as knockdown shRNA studies demonstrate that blocking VEGF or silencing *VEGFR2* inhibits the maturation of tumour endothelial progenitors into endothelium but not the differentiation of CD133$^+$ cells into endothelial progenitors, whereas γ-secretase inhibition or *NOTCH1* silencing blocks the transition into endothelial progenitors. These data may provide new perspectives on the mechanisms of failure of anti-angiogenesis inhibitors currently in use. The lineage plasticity and capacity to generate tumour vasculature of the putative cancer stem cells within glioblastoma are novel findings that provide new insight into the biology of gliomas and the definition of cancer stemness, as well as the mechanisms of tumour neo-angiogenesis.

Blood vessels within GBM express a variety of markers, including CD31 and CD105 (also known as PECAM1 and ENG, respectively); CD105 is a proliferation-associated molecule expressed in angiogenic endothelium[9]. Quantitative analysis of 16 GBM specimens by fluorescence-activated cell sorting (FACS) and immunohistochemistry showed that more than 70% of CD105$^+$ cells co-express CD31 (Fig. 1a, b), VEGFR2 (also known as KDR) and von Willebrand factor (also known as VWF), exhibit endothelial morphology, and labelling by DiI-AcLDL (1,1′-dioctadecyl-3,3,3′,3′-tetramethyl-indocarbocyanine perchlorate, ref. 10), suggesting an endothelial phenotype (Supplementary Fig. 1a). On average, ~5% of the total cell population expressed CD31 in normal brain and GBM specimens ($n = 7$), whereas CD105$^+$ cells were essentially absent in normal brain (Supplementary Fig. 1b). CD105$^+$ cells were also isolated by FACS from fresh GBM specimens and injected with a collagen matrix[11] into the flank of NOD-SCID mice. The resulting implants were composed of a network of vascular channels of human origin, expressed CD105 and CD31 and showed evidence of uptake of systemically injected lectin (Fig. 1c).

Whereas endothelial cells in GBMs are often classified as "hyperplastic"[2], the abnormal blood vessel architecture, the distinct gene expression profiles[12] and the selective emergence of abnormal vessels in GBMs versus lower grade gliomas[2] suggest a more complex ontogeny of GBM endothelium. We performed quantitative fluorescence *in situ* hybridization (FISH) analyses for *EGFR* and chromosome 7 (ref. 13) on CD105$^+$ cells isolated by FACS and on sections of the corresponding GBM parent tumour (Fig. 1d, e and Supplementary Fig. 2). The proportion of CD105$^+$ cells harbouring ≥3 copies of the *EGFR* amplicon or the centromeric portion of chromosome 7 was comparable to the proportion of tumour cells with the same aberrations (Supplementary Table 1a). We also performed quantitative PCR (qPCR) for three segments of the *EGFR* amplicon (exons 4, 9 and 11), known to be mutated at high frequency according to data from The Cancer Genome Atlas[6]. The data demonstrate a similar copy number in the CD105$^+$ cells and the corresponding parent tumour (Supplementary Table 1b) and indicate that a proportion of tumour endothelial cells within GBM is in fact neoplastic.

CD133 is a cell surface glycoprotein used extensively as a marker of putative cancer stem cells (CSCs) but also expressed in haematopoietic stem cells[14–18]. Although the specific identity and definition of CSCs remains a matter of debate, we proposed that the CD133$^+$ fraction may be related to the endothelial differentiation potential observed. Acutely dissociated cells from a series of 14 GBMs were fractionated into four groups: (1) CD144$^+$/CD133$^-$, (2) CD144$^+$/CD133$^+$ (double positive, DP), (3) CD133$^+$/CD144$^-$ and (4) CD133$^-$/CD144$^-$ (double negative, DN) (Fig. 2a). All samples contained the four fractions, with the DN being the largest population (Supplementary Table 4). Quantitative PCR with reverse transcription (qRT–PCR) analysis for endothelial markers (Supplementary Fig. 3a) demonstrated marked enrichment of *VEGFR2* and the endothelial progenitor marker *CD34* in the CD144$^+$/CD133$^-$ and in the DP populations. CD105 was consistently absent in the CD133$^+$ and CD144$^+$ fractions. To define lineage potential further, DP cells were cultured for 5 days in endothelial cell medium which resulted in the downregulation of CD144, the upregulation of CD105 and CD31 as well co-expression of VEGFR2 and CD34 and labelling with DiI-AcLDL (Fig. 2b and Supplementary Fig. 3b). When grown in three-dimensional (3D) gel cultures, the *in vitro* DP-derived endothelial cells form vascular networks reminiscent of normal endothelium, but also thickened channel walls and areas of confluence more suggestive of abnormal tumour vessels (Fig. 2c, d). The primary CD105$^+$ cells also form glomeruloid-like structures in 3D gel, with high lectin uptake (Supplementary Fig. 1c). DP-derived CD105$^+$ cells were sorted and injected subcutaneously in NOD/SCID mice, giving rise to

[1]Department of Neurosurgery, Memorial Sloan Kettering Cancer Center, New York, New York 10065, USA. [2]Center for Stem Cell Biology, Memorial Sloan Kettering Cancer Center, New York, New York 10065, USA. [3]Brain Tumor Center, Memorial Sloan Kettering Cancer Center, New York, New York 10065, USA. [4]Molecular Cytogenetics, Memorial Sloan Kettering Cancer Center, New York, New York 10065, USA. [5]Flow Cytometry Core, Memorial Sloan Kettering Cancer Center, New York, New York 10065, USA. [6]Neurosurgical Center Amsterdam, Academic Medical Center, Amsterdam 1105 AZ, The Netherlands. [7]Human Oncology and Pathogenesis Program, Memorial Sloan Kettering Cancer Center, New York, New York 10065, USA.

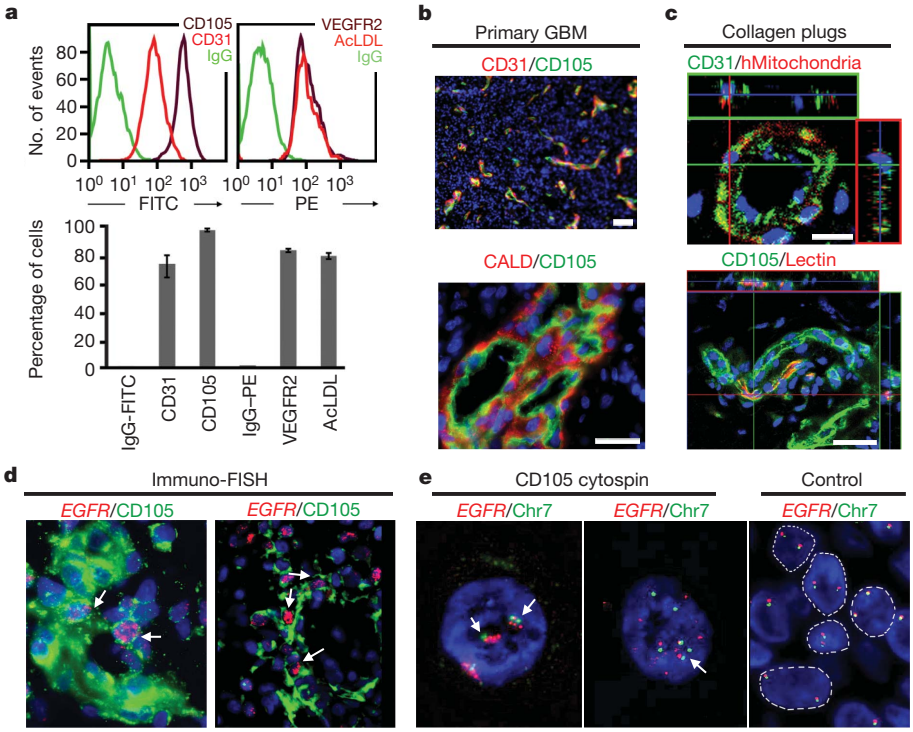

Figure 1 | CD105$^+$ endothelial cells in GBM harbour genomic aberrations. **a**, FACS analysis and quantification of GBM-derived CD105$^+$ cells shows co-expression of other endothelial cell markers (CD31, VEGFR2) and uptake of DiI-AcLDL($n = 3$). FITC, fluorescein isothiocyanate; PE, phycoerythrin **b**, CD105 immunostaining in GBMs delineates microvessels co-labelling with CD31 and glomeruloid vessels surrounded by caldesmon (CALD)-expressing pericytes. **c**, Functional neovessel formation by GBM-derived CD105$^+$ cells in the flank of NOD-SCID mice. Confocal immunofluorescence demonstrates co-localization of a human mitochondria marker with CD31 and uptake of lectin by the CD105$^+$ vessels in the implants. **d**, Immuno-FISH of CD105$^+$ vessels in GBM specimens (case 76, 78) shows multiple copies of the *EGFR* amplicon (arrows). **e**, FISH on CD105$^+$ cells sorted from GBMs confirms amplification of *EGFR* (red) and chromosome 7 centromere (Chr7, green) (arrows). Control nuclei, individually contoured, are from normal human fibroblasts. Scale bars, 50 μm. Error bars, s.d.

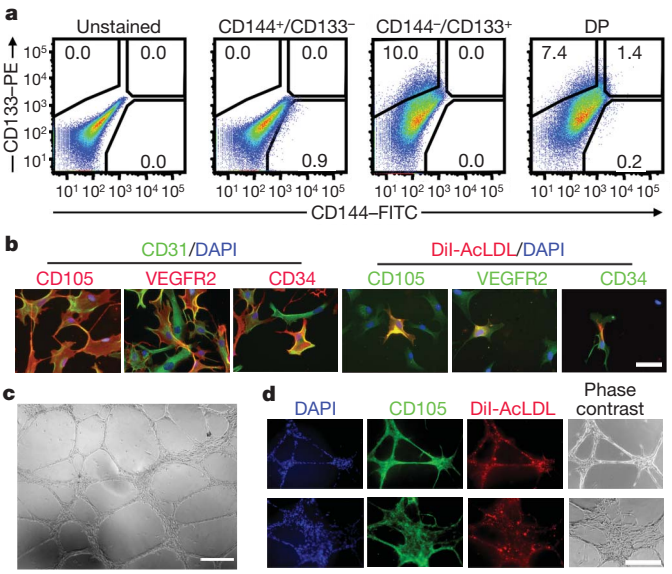

Figure 2 | GBM-derived CD133$^+$ cells include a fraction of endothelial progenitors **a**, Representative FACS analysis of a GBM specimen with fractionation into four cell subpopulations based on the expression of CD133 and vascular E-cadherin (CD144). **b**, Immunofluorescence analysis of DP (CD133$^+$/CD144$^+$) cells upon differentiation demonstrates co-expression of endothelial markers and DiI-AcLDL uptake. **c**, **d**, In Matrigel, DP cells will exhibit DiI-AcLDL uptake and form tubular networks comparable to those shown by normal endothelial cells, as well as areas of thickened walls where cells are more proliferative. Scale bars, 100 μm in **b** and **d**; 300 μm in **c**.

vascularized plugs identical to those obtained from primary CD105$^+$ cells (Supplementary Fig. 1d).

The CD144$^+$/CD133$^-$ cell fraction was often very small but showed a restricted differentiation and immunohistochemical profile (Supplementary Fig. 3c, d). When grown in Matrigel, the CD144$^+$/CD133$^-$ cells develop tubular, capillary-like structures[19] and no glomeruli (Supplementary Fig. 3e). CD144$^+$/CD133$^-$ cells do not express neural markers or form neurospheres, thus indicating a more restricted endothelial precursor cell identity (Supplementary Fig. 3f). Unsupervised clustering of transcriptome data was performed on several data sets including independent samples of the four sorted tumour subpopulations, as well as CD144$^+$ human embryonic stem-cell-derived endothelial precursors and bone-marrow-derived CD34$^+$ endothelial progenitors (Supplementary Fig. 3g). Taken together, these results indicate that GBMs comprise cell fractions capable of endothelial cell differentiation.

The identification of genomic aberrations in tumour endothelium and the presence of endothelial progenitors within the CD133$^+$ putative CSC fraction in GBMs, led us to postulate that DP cells may represent the neoplastic origin of tumour endothelium and could derive from the CD133$^+$ CSC fraction. CD133$^+$/CD144$^-$ cells were then labelled with *EFα-1::GFP* (elongation factor α1–green fluorescent protein) lentiviral vectors, triple sorted, and GFP$^+$/CD133$^+$/CD144$^-$ cells were co-cultured in the presence of tumour cells. On day 5, FACS analysis demonstrated the emergence of a GFP$^+$-DP population (Fig. 3a, b). When placed in collagen cultures, the GFP$^+$-DP cells had intracellular vacuoles suggestive of early lumen formation by endothelial tubes[20] (Fig. 3c), and differentiation into cells that express CD105 and CD31 and exhibit DiI-AcLDL uptake (Fig. 3d and Supplementary Fig. 4a). Importantly, co-culture with tumour cells is essential for the emergence of DP cells (Fig. 3a, b). Our data confirm that the DP endothelial

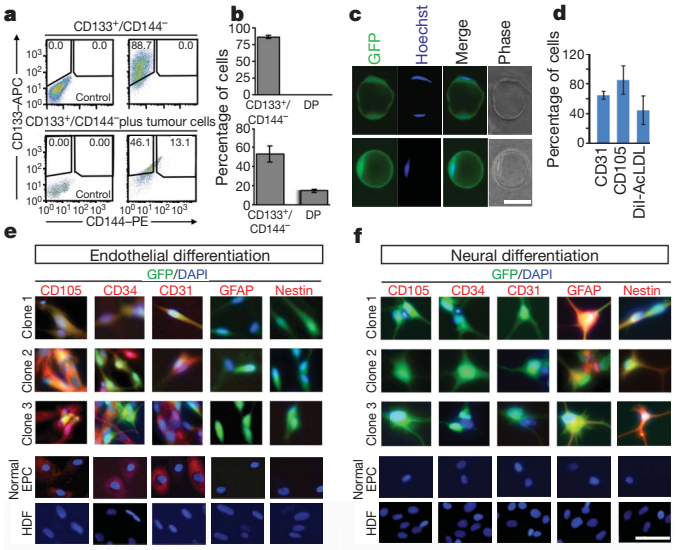

Figure 3 | CD133$^+$/CD144$^-$ cells are multipotential and give rise to endothelial cells via an endothelial progenitor intermediate. **a**, **b**, Co-cultures of CD133$^+$/CD144$^-$ cells with tumour cells give rise to endothelial progenitors that co-express CD133 and CD144 (DP) as shown and quantified by FACS analysis ($n = 3$). APC, allophycocyanin. **c**, GFP$^+$-derived DP cells form intracellular vacuolar structures in collagen gel, characteristic of endothelial cells. **d**, Immunohistochemistry of CD133$^+$/CD144$^-$-derived endothelial cells ($n = 3$). **e**, **f**, Single cell clonal analysis of GFP-labelled CD133$^+$/CD144$^-$ cells. GFP$^+$ clones derived from single cells are seeded under neural or endothelial conditions. Normal endothelial precursor cultures (EPC) and human dermal fibroblasts (HDF) were used as controls. Under endothelial conditions, all cells except HDF express endothelial but not neural markers. Under neural conditions, cells from the same GFP/CD133$^+$ clone are positive for GFAP and nestin but not endothelial markers, while controls are negative for all markers. Scale bar, 50 μm. Errors are s.d.

progenitors within GBM can arise from the CD133$^+$ cell population and are capable of differentiating into endothelial cells of tumour origin. Of note, the tumour cells used in these co-culture experiments originate from tumours with different genetic backgrounds and transcriptomal subclasses (Supplementary Tables 2 and 3).

Recent data support a close interaction[21] or a lineage relationship[22] between endothelial cells and neural stem cells. We next explored whether endothelial differentiation of CD133$^+$/CD144$^-$ can be further promoted by extrinsic signals. To this end, CD133$^+$/CD144$^-$ cells were isolated from GBM samples, stably transduced with *EFα-1::GFP* lentiviral vectors, sorted for GFP$^+$/CD133$^+$/CD144$^-$ and co-cultured with tumour-derived endothelial cells. GFP-expressing endothelial cells were identified at 7–10 days *in vitro* as demonstrated by co-labelling of GFP with CD105 and CD31, and also incorporation of DiI-AcLDL. Control experiments using GFP-labelled CD133$^-$ cells did not yield any endothelial cells (Supplementary Fig. 4b). The CD133$^+$/CD144$^-$ population formed neurospheres and readily differentiated along the three main CNS lineages (Supplementary Fig. 4c). Whereas these data are suggestive of the multipotent nature of the CD133$^+$/CD144$^-$ cells, they do not rule out the presence of heterogeneous populations within the CD133$^+$/CD144$^-$ fraction with distinct differentiation potentials. We thus performed single-cell clonal studies of CD133$^+$/CD144$^-$ cells as well as normal endothelial cells and fibroblasts as controls (Supplementary Fig. 4d). The data demonstrate both endothelial and neural differentiation potential within a single-cell derived clone confirming that CD133$^+$/CD144$^-$ cells are capable of generating tumour cells and tumour-derived endothelium (Fig. 3e, f). FISH for *EGFR* and chromosome 7 in the clones confirmed the presence of genomic amplifications identical to those exhibited by the parent tumour tissue (Supplementary Fig. 4e).

We next tested the fate of the various tumour cell fractions upon transplantation *in vivo*. CD133$^+$/CD144$^-$, DP, CD144$^+$/CD133$^-$ and DN cells were injected into the striatum of immunodeficient mice. All grafted animals developed tumours with the exception of those that received cells from the DN and CD144$^+$/CD133$^-$ fraction. DP and CD133$^+$/CD144$^-$ gave rise to large, highly infiltrative and hyperproliferative tumours showing strong expression of nestin (Fig. 4a). Whereas all xenograft tumours had a comparable volume and proliferation rate, the DP-derived tumours showed significantly increased levels of vascularization as demonstrated quantitatively (Supplementary Fig. 5a).

Some of the animals were grafted with stably GFP-marked CD133$^+$ cells allowing us to serially passage GFP-labelled CD133$^+$/CD144$^-$ cells from the primary xenograft in NOD-SCID mice. Secondary tumours formed at similar efficiency and showed comparable cell composition to the first passage cells. FACS analysis of GFP labelled xenograft cells demonstrates expression of endothelial markers, including CD105 and CD34 (Fig. 4b). After a second passage *in vivo*, tumours were sorted again for GFP$^+$/CD133$^+$/CD144$^-$ cells, which upon culture gave rise to GFP-labelled CD31$^+$ and CD105$^+$ cells, thus demonstrating maintenance of the multipotential phenotype (Fig. 4c). Immunohistochemical analysis, including confocal microscopy, demonstrated tumour blood vessels with typical morphology that express human markers. Tumour-bearing animals were also injected systemically with lectin, resulting in vessel-specific uptake and co-labelling with human markers (Fig. 4d, e and Supplementary Fig. 6). Thus, multipotency—including differentiation capacity along endothelial lineages—is maintained within the CD133$^+$/CD144$^-$ population *in vivo* and upon passaging. However, in the absence of clonal studies *in vivo*, true multipotency of tumour stem-like cells cannot be definitively confirmed.

A more comprehensive and quantitative analysis of genomic aberrations was conducted in order to verify the lineage relationship among the different tumour subpopulations. qPCR for the *EGFR* exons as described above[6] demonstrates the highest copy number within the CD133$^+$/CD144$^-$ population followed by the endothelial progenitors (DP) and the CD105$^+$ cells (Supplementary Fig. 5b). Interestingly, the CD31$^+$ cells and the CD144$^+$/CD133$^-$ progenitors showed lower levels of amplification, indicating that they may include a significant proportion of genotypically normal cells. We propose that these cells largely represent normal endothelium and circulating endothelial progenitors, respectively. This is compatible with the more restricted endothelial fate demonstrated by the CD144$^+$/CD133$^-$ cells as shown above (Supplementary Fig. 3c, e, f). Quantitative FISH studies for copy number of *EGFR* and chromosome 7 per cell were performed on CD133$^+$/CD144$^-$, DP and CD105$^+$ cells and revealed a substantial proportion of cells bearing the neoplastic aberrations in each population, ranging from 47.3% to 71.7% (Supplementary Fig. 5c). To address genomic alterations in tumour cells in a more unbiased manner we performed array comparative genomic hybridization (CGH) on the fractionated populations (Supplementary Fig. 7). The CGH data showed similar patterns of genomic aberrations in tumour cells as well as the endothelium and its progenitors, at variable amplitudes and across different regions, thus demonstrating a similar paradigm even in tumours that do not exhibit *EGFR* gain. We performed transcriptome analyses on a set of 18 tumours used in this study and found a random distribution of commonly described genotypes as well as representation of all TCGA-defined transcriptomal classes (Supplementary Table 3). Finally, we performed metaphase spreads on purified cell fractions of CD133$^+$/CD144$^-$, DP and CD105$^+$ following short-term culture. The majority of the cells had a highly abnormal but near-diploid karyotype, indicating that nuclear fusion is a very unlikely explanation for the lineage transition from cancer cell to endothelial progenitor or mature cell (Supplementary Fig. 5d). Vascular mimicry has been described in melanoma[23] and other tumours[24]; aneuploidy was also shown in renal cell cancer endothelium, but not matched to parent tumour cells[25].

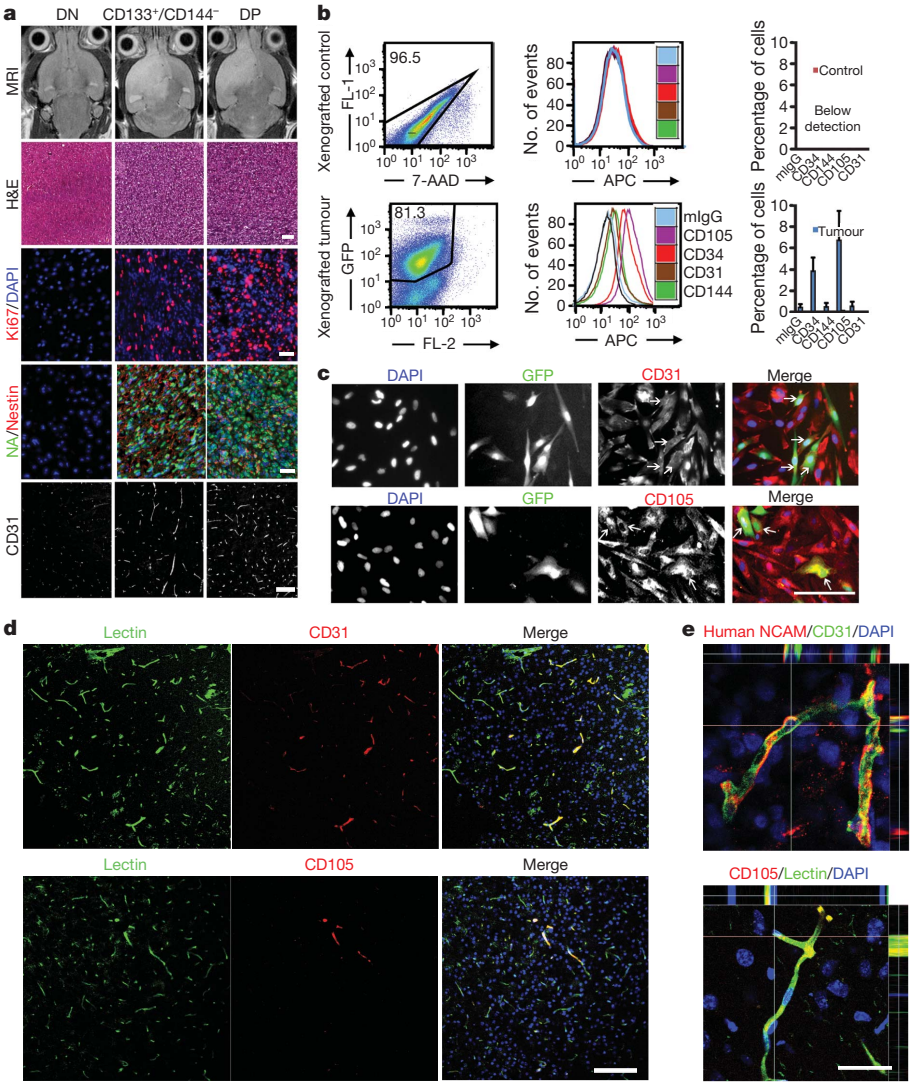

Figure 4 | Cancer stem-like cells and endothelial progenitors give rise to tumour and endothelial cells *in vivo*. **a**, Representative magnetic resonance imaging (MRI) images from mice that received injection of DN, $CD133^+/CD144^-$ or DP cells from primary GBM specimens. T2 sequences demonstrate infiltrative tumours except in the DN group. Tumours were hypercellular on haematoxylin and eosin (H&E), showed high proliferation rates (Ki67) and nestin expression. Immunostaining for human-specific CD31 demonstrates the presence of vessels of human origin within the tumours. NA, human nuclear antigen. **b**, FACS plots (left) and quantitative analysis (right) for endothelial marker expression in xenograft tumours ($GFP^+/CD133^+/CD144^-$ cells) and controls (DN). ($n = 3$, s.d.). 7-AAD, 7-aminoactinomycin. FL-1 and 2, fluorescent channels 1 and 2; mIgG, mouse immunoglobulin G. **c**, Xenograft derived $GFP^+/CD133^+/CD144^-$ cells express endothelial markers upon *in vitro* differentiation (arrows). **d**, Uptake of systemic lectin in tumour xenografts demonstrates blood vessels that co-label with human endothelial markers (CD31 and CD105). **e**, Confocal microscopy of xenograft microvasculature. Scale bars, 100 μm in **a**; 50 μm in **c**; 140 μm in **d**; 10 μm in **e**.

We investigated the impact of DAPT (N-[N-(3,5-difluorophenacetyl)-L-alanyl]-*S*-phenylglycine *t*-butyl ester), a γ-secretase inhibitor that effectively inhibits Notch signalling[8], and bevacizumab, a VEGFA-binding antibody[7] currently in clinical use, on the differentiation of $CD133^+/CD144^-$ to DP and then to $CD105^+$ cells. Exposure to bevacizumab did not have an impact on the ability of $CD133^+/CD144^-$ cells to differentiate into endothelial progenitors, yet it blocked further maturation from DP into $CD105^+$ endothelial cells. In contrast, γ-secretase inhibition resulted in significant suppression of the transition from $CD133^+/CD144^-$ to DP, but did not affect maturation to $CD105^+$ cells. To demonstrate the specific roles of the Notch and VEGF pathways, we performed knockdown studies targeting the *NOTCH1* and *VEGFR2* receptors. The gene silencing data further supported the results of the inhibitor studies (Supplementary Figs 8b and 9). Gene expression analysis shows significant upregulation of *NOTCH1/2* and *VEGFR1/2* in the $CD133^+/CD144^-$ and DP groups, respectively (Supplementary Fig. 8). These preliminary studies offer a novel perspective of the roles of the VEGF and Notch pathways in glioma biology, although the functional consequences of VEGF or Notch blockade remain to be determined.

Despite some promise, bevacizumab therapy is often interrupted by GBM progression characterized by a decrease in abnormal vascularity and significant invasive tumour behaviour[26]. Based on the paradigm presented here (Supplementary Fig. 9a), bevacizumab failure could be conceivably due to the disruption of the dynamic relationships between the tumour fractions.

In summary, our data demonstrate that a subpopulation of cells within GBM can give rise to endothelial cells via a bipotential progenitor intermediate, and that the $CD133^+$ cancer stem-cell-like fraction includes a population of endothelial progenitors. An in-depth understanding of the lineage relationship between tumour cells and endothelial progeny should provide new insights into CSC biology and tumour self-renewal. Given the strong correlation of tumour grade and neoplastic vasculature in human gliomas, agents that could block endothelial

transition of tumour cells may provide a novel therapeutic strategy for this currently intractable disease.

METHODS SUMMARY

All experiments were conducted on freshly obtained surgical specimens of glioblastoma tumour; a neuropathologist confirmed the diagnosis on frozen section before tissue acquisition. Tumours were newly diagnosed or recurrent. A total of 78 tumours were used in the study. Cell fractions were sorted using standard methods at our FACS facility; *in vitro* experiments were conducted on short-passage cultures (maximum of five passages) if needed. A total of 34 xenografts were obtained in immunodeficient mice following intrastriatal implantation of cell populations as indicated in the Methods. A lentiviral vector expressing GFP under a PGK promoter (gift from M. Sadelain) was used for cell labelling and sorting. Cytogenetic analyses were conducted using standard methods at the Cytogenetics Core facility at Sloan Kettering Cancer Center. Knockdown experiments were performed using lentiviral vectors expressing shRNA for *NOTCH1* or *VEGFR2* (Santa Cruz). All experiments were carried out in triplicates or greater. Data are expressed as mean ± s.d. P values were determined following two-tailed student's t-test. A P value of <0.05 was considered significant. Tissues were obtained after patients' written consent under a protocol approved by the institution's Institutional Review Board.

Full Methods and any associated references are available in the online version of the paper at www.nature.com/nature.

Received 10 May; accepted 1 November 2010.

Published online 21 November 2010.

1. Stupp, R. *et al.* Radiotherapy plus concomitant and adjuvant temozolomide for glioblastoma. *N. Engl. J. Med.* **352,** 987–996 (2005).
2. Kleihues, P. *et al.* The WHO classification of tumors of the nervous system. *J. Neuropathol. Exp. Neurol.* **61,** 215–225 (2002).
3. Kioi, M. *et al.* Inhibition of vasculogenesis, but not angiogenesis, prevents the recurrence of glioblastoma after irradiation in mice. *J. Clin. Invest.* **120,** 694–705 (2010).
4. Lyden, D. *et al.* Impaired recruitment of bone-marrow-derived endothelial and hematopoietic precursor cells blocks tumor angiogenesis and growth. *Nature Med.* **7,** 1194–1201 (2001).
5. Du, R. *et al.* HIF1alpha induces the recruitment of bone marrow-derived vascular modulatory cells to regulate tumor angiogenesis and invasion. *Cancer Cell* **13,** 206–220 (2008).
6. The Cancer Genome Atlas Research Network. Comprehensive genomic characterization defines human glioblastoma genes and core pathways. *Nature* **455,** 1061–1068 (2008).
7. Kreisl, T. N. *et al.* Phase II trial of single-agent bevacizumab followed by bevacizumab plus irinotecan at tumor progression in recurrent glioblastoma. *J. Clin. Oncol.* **27,** 740–745 (2009).
8. Hovinga, K. E. *et al.* Inhibition of Notch Signaling in Glioblastoma Targets Cancer Stem Cells Via an Endothelial Cell Intermediate. *Stem Cells* **28,** 1019–1029 (2010).
9. Dallas, N. A. *et al.* Endoglin (CD105): a marker of tumor vasculature and potential target for therapy. *Clin. Cancer Res.* **14,** 1931–1937 (2008).
10. Voyta, J. C., Via, D. P., Butterfield, C. E. & Zetter, B. R. Identification and isolation of endothelial cells based on their increased uptake of acetylated-low density lipoprotein. *J. Cell Biol.* **99,** 2034–2040 (1984).
11. Laib, A. M. *et al.* Spheroid-based human endothelial cell microvessel formation *in vivo*. *Nature Protocols* **4,** 1202–1215 (2009).
12. Beaty, R. M. *et al. PLXDC1* (*TEM7*) is identified in a genome-wide expression screen of glioblastoma endothelium. *J. Neurooncol.* **81,** 241–248 (2007).
13. Verhaak, R. G. *et al.* Integrated genomic analysis identifies clinically relevant subtypes of glioblastoma characterized by abnormalities in *PDGFRA*, *IDH1*, *EGFR*, and *NF1*. *Cancer Cell* **17,** 98–110 (2010).
14. Singh, S. K. *et al.* Identification of human brain tumour initiating cells. *Nature* **432,** 396–401 (2004).
15. Richardson, G. D. *et al.* CD133, a novel marker for human prostatic epithelial stem cells. *J. Cell Sci.* **117,** 3539–3545 (2004).
16. Al-Hajj, M., Wicha, M. S., Benito-Hernandez, A., Morrison, S. J. & Clarke, M. F. Prospective identification of tumorigenic breast cancer cells. *Proc. Natl Acad. Sci. USA* **100,** 3983–3988 (2003).
17. Shmelkov, S. V., St, C. R., Lyden, D. & Rafii, S. AC133/CD133/Prominin-1. *Int. J. Biochem. Cell Biol.* **37,** 715–719 (2005).
18. Uchida, N. *et al.* Direct isolation of human central nervous system stem cells. *Proc. Natl Acad. Sci. USA* **97,** 14720–14725 (2000).
19. Koh, W., Mahan, R. D. & Davis, G. E. Cdc42- and Rac1-mediated endothelial lumen formation requires Pak2, Pak4 and Par3, and PKC-dependent signaling. *J. Cell Sci.* **121,** 989–1001 (2008).
20. Kamei, M. *et al.* Endothelial tubes assemble from intracellular vacuoles *in vivo*. *Nature* **442,** 453–456 (2006).
21. Shen, Q. *et al.* Endothelial cells stimulate self-renewal and expand neurogenesis of neural stem cells. *Science* **304,** 1338–1340 (2004).
22. Wurmser, A. E. *et al.* Cell fusion-independent differentiation of neural stem cells to the endothelial lineage. *Nature* **430,** 350–356 (2004).
23. Hendrix, M. J. *et al.* Transendothelial function of human metastatic melanoma cells: role of the microenvironment in cell-fate determination. *Cancer Res.* **62,** 665–668 (2002).
24. El Hallani, S. *et al.* A new alternative mechanism in glioblastoma vascularization: tubular vasculogenic mimicry. *Brain* **133,** 973–982 (2010).
25. Akino, T. *et al.* Cytogenetic abnormalities of tumor-associated endothelial cells in human malignant tumors. *Am. J. Pathol.* **175,** 2657–2667 (2009).
26. Iwamoto, F. M. *et al.* Patterns of relapse and prognosis after bevacizumab failure in recurrent glioblastoma. *Neurology* **73,** 1200–1206 (2009).

Supplementary Information is linked to the online version of the paper at www.nature.com/nature.

Acknowledgements We would like to thank J. Imai, H. Xu, G. Lee, M. Tomishima and L. Studer for critical reading of the manuscript, P. Gutin for assistance with tissue acquisition and discussions, B. Weksler for the brain endothelial cell line (hCMEC), S. Jhanwar for the clinical cytogenetics data and M. Sadelain and E. Papapetrou for the lentiviral vectors. Funding was provided in part through a grant from the New York State Stem Cell Science Fund (NYSTEM).

Author Contributions R.W. and V.T. conceived the project, analysed the data and wrote the manuscript. R.W. and remaining authors performed experiments and analysed data.

Author Information Microarray and CGH data are deposited in NCBI's Gene Expression Omnibus (GSE24244, GSE24446, GSE24452, GSE24557 and GSE24558). Reprints and permissions information is available at www.nature.com/reprints. The authors declare no competing financial interests. Readers are welcome to comment on the online version of this article at www.nature.com/nature. Correspondence and requests for materials should be addressed to V.T. (tabarv@mskcc.org).

METHODS

Tissue processing. Surgical specimens were collected from the surgical suite at Memorial Sloan Kettering Cancer Center, following diagnostic confirmation by a neuropathologist. Tissues were obtained after patients' written consent under a protocol approved by the institution's Institutional Review Board. Tumours were cut mechanically first (McIlwain Tissue Chopper) then dissociated into single cells with Liberase Blendzyme 1 (Roche) as described previously[27].

Single cells were blocked with human FcR (1:20, Miltenyi Biotec) at 4 °C for 20 min before incubation with primary antibodies for 30 min. Cells from xenografts were further blocked with 2,4-G2 (1:100; Santa Cruz Biotechnology) before incubation with antibodies. Cells were incubated with primary antibodies, washed and reincubated with appropriate secondary antibodies and resuspended in FACS buffer[27] (containing 1× $Ca2^{+}/Mg2^{+}$-free HBSS (Invitrogen), 10 mM of HEPES, 0.156% of glucose and 0.5% of low endotoxin BSA fraction V, all from Sigma (Sigma-Aldrich), at a pH of 7.2) with 1 μg ml^{-1} 7-aminoactinomycin D (7-AAD, BD Pharmingen) before analysis. Mouse IgG1 or secondary antibody alone served as control for unspecific binding. Samples were analysed on a FACS Aria flow cytometer with CellQuest software (BD Biosciences) and data were analysed using FlowJo software (Tree star). A minimum of 10,000 events were counted and cell surface expression was analysed in 7-AAD-negative live cells. Antibodies used include: phycoerythrin- or allophycocyanin-conjugated anti-CD133 (1:20, Miltenyi Biotec); FITC-conjugated anti-CD144 (1:20, Abcam), anti-CD105 (1:20, BD Biosciences) and anti-CD31 (1:20, BD Biosciences); mouse anti-human CD31 (1: 40; BD Biosciences), mouse anti-human CD105 (1:40; Dako), mouse anti-human VEGFR2 (1:40; Abcam), mouse anti-human CD34 (1:20; Abcam), mouse anti-human CD144 (1:20; Abcam); mouse anti-human CD133 antibodies (AC141 and AC133 epitopes (1:20 each), Miltenyi). FITC-conjugated lectin and tetramethyl rhodamine isothiocyanate (TRITC)-conjugated lectins were purchased from Vector and Sigma separately.

DNA and RNA preparation. FACS-sorted cell populations from 21 glioblastoma patients were used to extract total RNA using an Absolutely RNA Nanoprep kit (Stratagene) or an RNeasy Kit (Qiagen). All RNA samples were pre-treated with DNase. Sorted cell populations from eight glioblastoma patients were used to isolate genomic DNA using the Picopure DNA extraction kit (Molecular Devices), followed by phenol (Invitrogen) extraction.

***In vivo* studies.** Adult female NOD/SCID or male NOD/SCID gamma (NSG) mouse (Jackson Laboratory) were anaesthetized with ketamine/xylazine (Hospira) and placed in a stereotaxic frame (Stoelting Company). Freshly sorted cells were injected into the right striatum immediately after sorting at the following coordinates (relative to bregma): AP = +0.5, ML = −2, and DV = −2.7. Animals received 10,000 cells each of $CD133^{+}/CD144^{-}$, $CD133^{-}/CD144^{+}$ or DP. NSG mice received 500 cells each of $CD133^{+}/CD144^{-}$ or DP. DN cells were used in three separate doses (10,000, 50,000 and 100,000 cells). Animals were killed upon exhibiting symptoms. Some animals received FITC-conjugated lectin by retro-orbital injection before killing. Total animals grafted $n = 40$.

The gel implantation assay was modified from ref. 11. Briefly, GBM- or DP-derived $CD105^{+}$ (10^6 or 2×10^6 per ml) were resuspended in Collagen IV (Chemicon). GBM- or DP-derived cell-gel suspension (500 μl) was injected subcutaneously below the xiphoid in four or three mice separately. Some animals received TRITC-conjugated lectin by tail vein injection before killing. After transplantation (21 days) the implants were retrieved, fixed overnight in 4% (v/v) buffered formalin at 4 °C, embedded in Optimal Cutting Temperature Compound (O.C.T. compound, Sakura Finetek) and sectioned on a freezing cryostat (Leica) for histological examination. Animals were housed and cared for in accordance with the National Institutes of Health (NIH) guidelines for animal welfare and all animal experiments were performed in accordance with protocols approved by our Institutional Animal Care and Use Committee (IACUC).

Animal imaging. *In vivo* magnetic resonance imaging was performed on a Bruker Biospec 4.7-Tesla 40-cm horizontal bore magnet. The system is equipped with a 200 mT m^{-1} gradient system. Examinations were conducted using a 72-mm birdcage resonator for excitation, and detection was achieved using a 3 cm surface coil. T2-weighted spin echo images were acquired consecutively using a rapid-acquisition relaxation enhanced sequence (RARE). Animals were anesthetized with 2% isoflurane in N_2/O_2 mixture.

Immunofluorescence. Primary antibodies were chicken anti-GFP (1:1,000; Chemicon), mouse anti-human CD31 (1:400; Abcam); mouse anti-human CD34 (1:400; Abcam), mouse anti-human CD105 (1:400; Dako); mouse anti-human vWF (1:100; Dako); mouse anti-human VEGFR2 (1:200; Abcam); mouse anti-human Ki67 (1:400; Dako); mouse anti-human NCAM (1:150; Santa cruz Biotechnology), mouse anti-human mitochondria (1:200; Chemicon), mouse anti-human nestin (1:400; Millipore), mouse anti-human nuclear antigen (1:500; Chemicon), rabbit anti-human GFAP (1:1,000; Chemicon), mouse anti-human Tuj1 (1:500; Covance), mouse anti-O4 (1:200; Chemicon), rabbit anti-human caldesmon (1:400; Novus Biology). The following secondary antibodies were used: Alexa Fluor 488-conjugated goat anti-chicken or mouse or rabbit (1:1,000), Alexa Fluor 555-conjugated goat anti-mouse or rabbit (1:1,000), Alexa Fluor 555-conjugated goat anti-mouse IgM (1:500), all from Molecular Probes (Invitrogen).

Cell culture and clonal assays. GFP labelling was obtained by incubation with a PGK-GFP lentiviral vector (gift from M. Sadelain). For sphere cultures, freshly sorted $CD133^{+}/CD144^{-}$, DP and $CD133^{-}/CD144^{+}$ cells were cultured under clonal conditions (1,000 cells per cm^2 or 5 cells per μl) in low-adherence plates (Corning) and maintained in serum free-Neurobasal medium supplemented with N2 (Invitrogen), 2 mM L-glutamine, 20 ng ml^{-1} recombinant human epidermal growth factor, and 10 ng ml^{-1} recombinant human fibroblast growth factor 2 (all from Invitrogen). Neurospheres were reseeded every 5 days after dissociation with Accutase (Innovative Cell Technologies). For neural differentiation, $CD133^{+}/CD144^{-}$ cells were cultured in laminin coated plates (BD Biosciences) using NeuroCult NS-A Differentiation Kit (human) (Stem Cell Technologies).

For endothelial progenitor cells, freshly sorted DP or $CD144^{+}/CD133^{-}$ cells were seeded on human fibronectin-coated plates (BD Biosciences) at a density of 10^5 ml^{-1} with endo-cult liquid medium Kit (Stem Cell Technologies) for propagation. DP, $CD144^{+}/CD133^{-}$ or $CD133^{+}/CD144^{-}$-derived DP cells were grown to 75% confluence and switched to M199 medium (Invitrogen) for quantification of endothelial differentiation as described previously[19]. GBM-derived $CD105^{+}$ cells were grown in M199 medium[19] for 2 days before FACS analysis. The functional assay for endothelial cells was performed by incubation of cells with 10 μg ml^{-1} of DiI-labelled acetylated low density lipoproteins (DiI-AcLDL) (Molecular Probes, Invitrogen) for 4 h.

For DP induction culture, GFP-labelled $CD133^{+}/CD144^{-}$ were co-cultured with tumour cells at a 20:1 ratio in N2 medium. The $CD133^{+}/CD144^{-}$-derived DP cells were sorted by FACS after 5 days for further characterization. A minimum of 100 cells were counted in triplicate assays. They were cultured in three-dimensional collagen gel[20]. For differentiation of $CD133^{+}/CD144^{-}$ to endothelial cells, tumour endothelial cells and GFP labelled $CD133^{+}/CD144^{-}$ cells or control cells were resuspended in endo-cult medium and grown on fibronectin coated plates for 7 days at a ratio of 100:1. Single cell clonal assays were performed by seeding freshly sorted single GFP-labelled cells on multi-well plates. Wells containing single green cells were identified and monitored until clone formation is established. Single-cell-derived clones were further sub-cloned and propagated twice, dissociated and seeded under neural and endothelial differentiation conditions as described above. Human umbilical cord-derived $CD133^{+}$ endothelial precursor cells (Biochain) or human dermal fibroblasts (Cell Applications) were maintained as per manufacturer instructions and used as control in clonal analysis.

Inhibitor studies. For drug treatment assays, cells were cultured in DP induction medium or endothelial differentiation medium containing 5 μM of the γ-secretase inhibitor DAPT (N-[N-(3,5-difluorophenacetyl)-L-alanyl]-*S*-phenylglycine *t*-butyl ester, Sigma-Aldrich) or 1 μg $μl^{-1}$ of bevacizumab (Genentech). Treated cells were analysed by FACS analysis after 48 h incubation. VEGF was measured in the culture medium with a human VEGF ELISA Kit (Invitrogen) following the manufacturer directions.

Knockdown studies. GBM-derived fresh DP and GFP-CD133sp cells were infected with shRNA virus targeting *VEGFR2* or *NOTCH1* or a control virus (all from Santa Cruz Biotechnology). NOTCH1 shRNA lentiviral vector mix contains three target-specific constructs: CACCAGTTTGAATGGTCAATTCAA GAGATTGACCATTCAAACTGGTGTTTTT; CCCATGGTACCAATCATGA TTCAAGAGATCATGATTGGTACCATGGGTTTTT; CCATGGTACCAATC ATGAATTCAAGAGATTCATGATTGGTACCATGGTTTTT. VEGFR2 shRNA lentiviral vector mix contains three target-specific constructs: ACTGTGGTGATT CCATGTCTTCAAGAGAGACATGGAATCACCACAGTTTTTT; ACTTGTAA ACCGAGACCTATTCAAGAGATAGGTCTCGGTTTACAAGTTTTTT; CACC TGTTTGCAAGAACTTTTCAAGAGAAAGTTCTTGCAAACAGGTGTTTTT. The infected cells were selected with 2–4 μg ml^{-1} puromycin (Santa Cruz Biotechnology) and used for FACS analysis and/or collected for RT–PCR as described above after 5 days in selection.

***In vitro* angiogenesis assay.** Intracellular vacuole formation was evaluated by culturing $CD133^{+}/CD144^{-}$-derived DP cells in three-dimensional collagen gel as described in ref. 20. Tubular network formation was assessed by culture in growth factor reduced Matrigel assay Kit (BD Biosciences) following the protocol from ref. 19.

Cytogenetic analyses and genomic PCR. Fluorescence *in situ* hybridization was performed using BAC clone RP11-339F13 and PAC clone RP5-1091E12 spanning the *EGFR* locus in 7p11, both labelled with Red-dUTP, together with a chromosome 7 centromere repeat DNA probe labelled with Green-dUTP targeted at the centromeric region of chromosome 7 (7p11.1–7q11.1 D7Z1 alpha satellite region). FISH was performed on sorted cells post cytospin on glass slides. A minimum of 100 cells in interphase were analysed. Human dermal fibroblasts

(HDF) served as normal control. The false positive rates for FISH probes was determined as 1% (s.d. = 1.3) and the cut-off level for the diagnosis of amplification was set at 5% (>3s.d.) ($n = 3$, total counted 2,000 control cells).

FISH on tumour sections, as reported in Supplementary Tables 1b and 2, was performed independently by the Clinical Cytogenetics Facility at Memorial Sloan Kettering Cancer Center, as part of a now routine molecular diagnostic test. The probe used is the 7p12 LSI EGFR and the 7p11.1–7q11.1 CEP (D7Z1 alpha satellite) dual colour probe, purchased from Abbott Molecular.

Fluorescence immunophenotyping and interphase cytogenetics, a technique combining immunohistochemistry for CD105 and FISH for *EGFR*, was carried out on 10-μm thick tissue sections. Normal human brain cerebral-cortex sections (Biochain) were used as controls.

In a copy number quantification reaction by real-time PCR, *EGFR* primers were designed based on published data[6,28,29,30]. Genomic DNA (10 ng) from sorted cells or normal human brain was used as template to examine the copy number of exons 4, 9, 11 in the *EGFR* gene; *GAPDH* was used as reference gene. Each replicate was normalized to *GAPDH* to obtain a ΔC_t, and then an average ΔC_t value for each sample (from the three replicates) was calculated. All samples were then normalized to the calibrator sample (normal human brain) to determine $\Delta\Delta C_t$. Relative quantity (RQ) is $2^{\Delta\Delta Ct}$, and copy number is $2 \times$ RQ. The EGFR copy number in each population was defined by the average of copy number from three exons. Error bars indicate the range of the data from the three exons in each of the three samples.

Karyotype analysis was performed on metaphase spread of FACS-purified cell subpopulations that were in culture for 3 days. The cultures were treated with Colcemid (0.1 μg ml^{-1}) for 1.5 h before *in situ* metaphase preparation according to standard cytogenetics procedures.

CGH studies. Comparative genomic hybridization (CGH) assay was performed by hybridizing genomic DNA from sorted cells with 44K human genome CGH arrays, and frozen banked whole tumour on 244K and 1M human genome CGH arrays (all commercial arrays from Agilent). DNA from sorted cells was prepared as described above. DNA extraction, purification, labelling and hybridization were performed at Sloan Kettering Cancer Center's Genomics Core Facility according to the manufacturer's instructions. Log_2 ratios were normalized by Lowess against probe intensity and mean %GC of the genomic region mapped to by the probe. Segmentation of normalized log_2 ratios was by Circular Binary Segmentation (CBS, R package DNAcopy).

A separate method was used to investigate whether an amplicon identified by CBS in one cell fraction might be present in a minor subpopulation in other cell fraction at a level not detected by CBS. A region of interest (ROI) is defined by the boundaries of the amplicon detected by CBS. Then this region is investigated in the CGH profiles of the other cell fractions as follows: the log_2 ratios of the N probes under the ROI (within amplicon boundaries) are compared to log_2 ratios of all the other probes in the entire chromosome by Student's t-test (one-tailed). The observed t-score is then compared to the distribution of t-scores obtained by equivalently testing all other sets of N neighbouring probes in the chromosome. The ROI is considered to be significantly gained if the observed t-score is seen or exceeded in less than 0.1% of all other chromosomal regions.

Expression microarray studies of whole tumours. Gene expression profiling was performed for a subset of 16 tumours for which additional frozen material was available using exon expression arrays (Human Exon 1.0, Affymetrix). RNA was extracted, labelled and hybridized at Sloan Kettering Cancer Center's Genomics Core Facility according to the manufacturer's instructions. Data was normalized in a cohort of 80 gliomas using Aroma.affymetrix (R package aroma.affymetrix). Expression was derived for RefSeq transcripts, and multiple transcripts for the same gene were distilled to a single gene expression value by median. Transcriptomal class assignment was based on the nearest centroid of the four transcriptomal classes reported in ref. 13, using the subset of 840 signature genes described by this study (Supplementary Table 6; http://tcga-data.nci.nih.gov/docs/publications/gbm_exp/). Distances to centroids were defined using Pearson correlation and class assignments made by the largest correlation value. If the largest correlation was <0.2, the sample was labelled 'indeterminate'. Correlations and class assignments are given in Supplementary Table 6.

Microscopic analysis. Sections were examined with confocal laser scanning microscopy (Leica Microsystems; Carl Zeiss MicroImaging). The data was analysed with Velocity or LSM5 (Carl Zeiss MicroImaging) software.

Tumour microvessel density (MVD) was assessed by quantification of the numbers of $CD31^+$ tumour vessels in pixels using MetaMorph (Molecular Devices) image analysis software using unbiased sampling.

Gene expression analysis and quantitative real-time PCR for sorted cell populations. Total RNA of four subpopulations from two specimens were hybridized with human U133-plus2 array at Sloan Kettering Cancer Center's Genomics Core Facility and according to the manufacturer's instructions. Reference databases, including one set of $CD34^+$ human haematopoietic progenitor cells (GSM476781) and two independent sets of human embryonic stem cell-derived endothelial progenitors (GSM492830 and GSM492828) were downloaded from Gene Expression Omnibus database. The array data are analysed by Partek software. The data from 11 samples were normalized by RMA algorithms and the tumour samples then assigned in four groups based on the expression of membrane markers CD133 and CD144. The gene list is created by ANOVA with unadjusted P value less than 0.05 and then used as input for unsupervised hierarchical clustering by using Euclidian similarity metric.

For RT–PCR, total RNA (100–300 ng) was reverse-transcribed using random-primer and superscript III (Invitrogen) according to the manufacturer's instructions. Quantitative real-time PCR was performed with an Applied Biosystems Prism 7900HT sequence Detection System using SYBR Green PCR Master Mix (Applied Biosystems).

Primers: *CD34* (F: TCTGATCTCCATGGCTTCCT; R: ACTGAGGCAACAG CTCAACC), *CD144* (F: TCGTCATGGACCGAGGTT; R: TCTACAATCCCTT GCAGTGTGA), *VEGFR2* (F: GCAGGGGACAGAGGGACTTG; R: GAGGCC ATCGCTGCACTCA), *CD31* (F: TTCCTGACAGTGTCTTGAGTGG; R: GCT AGGCGTGGTTCTCATCT), *CD133* (F: TCTGGGTCTACAAGGACTTTCC; R: GCCCGCCTGAGTCACTAC), *ACTIN* (F: GCCCGCCTGAGTCACTAC; R: GGAATCCTTCTGACCCATGC), *VEGFR1* (F: TCTCACATCGACAAACCA ATACA; R: GGTAGCAGTACAATTGAGGACAAGA), *VEGF* (F: CTACCTCC ACCATGCCAAGT; R: CCACTTCGTGATGATTCTGC).

Human angiogenesis PCR arrays (SABiosciences) were used to examine the expression profiles of angiogenic genes in sorted cell populations. Heat Map construction and analysis of qPCR data was conducted according to ref. 31.

27. Panchision, D. M. *et al.* Optimized flow cytometric analysis of central nervous system tissue reveals novel functional relationships among cells expressing CD133, CD15, and CD24. *Stem Cells* **25,** 1560–1570 (2007).
28. Franco-Hernandez, C. *et al.* Gene dosage and mutational analyses of EGFR in oligodendrogliomas. *Int. J. Oncol.* **30,** 209–215 (2007).
29. Mellinghoff, I. K. *et al.* Molecular Determinants of the response of glioblastomas to EGFR kinase inhibitors. *N. Engl. J. Med.* **353,** 2012–2024 (2005).
30. Brennan, C. *et al.* Glioblastoma subclasses can be defined by activity among signal transduction pathways and associated genomic alterations. *PLoS ONE* **4,** e7752 (2009).
31. Guo, P. *et al.* Dual nature of the adaptive immune system in lampreys. *Nature* **459,** 796–801 (2009).